JOURNAL OF CATALYSIS **172,** 380–390 (1997)
ARTICLE NO. CA971859

Photocatalytic Reactions Involving Hydroxyl Radical Attack

II. Kinetics of the Decomposition of Trichloroethylene Using Titanium Dioxide

María I. Cabrera, Antonio C. Negro, Orlando M. Alfano, and Alberto E. Cassano[1]

Instituto de Desarrollo Tecnológico para la Industria Química (INTEC), Universidad Nacional del Litoral (U.N.L.) and Consejo Nacional de Investigaciones Científicas y Técnicas (CONICET), Güemes 3450, (3000) Santa Fe, Argentina

Received January 13, 1997; revised August 4, 1997; accepted August 5, 1997

The intrinsic reaction kinetics of the decomposition of trichloroethylene in water employing suspended titanium dioxide catalytic particles have been studied using near ultraviolet polychromatic radiation. Experiments were carried out in a one-dimensional one-directional reactor placed inside the loop of a batch recycling system (1, Cabrera, *et al.***,** *Ind. Eng. Chem. Res.* **33, 3031 (1994); 2, Alfano,** *et al.***,** *Ind. Eng. Chem. Res.* **34, 488 (1995)). Initial concentration of trichloroethylene was in the range of 0.15×10^{-6} to 0.75×10^{-6} mol cm^{-3} while catalyst concentration was varied from 0.1×10^{-3} to 1.0×10^{-3} g cm^{-3}. Oxygen concentration was always in excess of the stoichiometric demand. Results were analyzed in terms of a reaction model previously developed in Part I (3, Alfano,** *et al.***,** *J. Catal.* **172, 370 (1997)). According to the resulting kinetic expression therein, the values of the kinetic constant are: $\alpha_1 = 2.46 \times 10^{-8}$ mol cm^{-2} s^{-1}; $\alpha_2 = 1.57 \times 10^{11}$ g s einstein^{-1}; $\alpha_{3,i} = 6.42 \times 10^{6}$ cm^3 mol^{-1}.**

I. INTRODUCTION

Photocatalysis is the result of combining heterogeneous photochemistry with a solid catalytic process that usually employs suspended or immobilized metal oxide semiconductor particles (4, 5). Ultraviolet light of the appropriate wavelength is used to excite the semiconductor and, upon photoactivation, electrons (in the conduction band) and holes (in the valence band) become available. Afterwards, both species can interact with the gas or the liquid phase surrounding environment. These subsequent reactions may involve different substances and intermediates via a complex redox mechanism that is believed to involve adsorbed species on the catalytic surface (for example, hydroxyl radicals, organic substrates, reaction intermediates). However, it is also known that apparent reaction kinetic results can be equally explained even if the reacting species are in the bulk of the fluid (6).

A large group of oxidative reactions occurring in these photocatalytic processes are analyzed in terms of a hydroxyl radical attack on a C–H bond. On this basis Turchi and Ollis (6) proposed a simplified, but complete and consistent, reaction sequence to interpret the observed kinetics. In Part I, Alfano *et al.* (3) developed an extension of such work incorporating a somewhat more general view of the hydroxyl attack. Also, and more important, this approach includes a detailed and rigorous treatment of the radiation energy absorption effects based on the proper solution of the radiative transfer equation (RTE).

Within the list of undesired water pollutant compounds, several halocarbons stand out due to their toxicity and persistence. Trichloroethylene (TCE) is one of these priority pollutants. The decomposition of trichloroethylene in water solution has been studied by Pruden and Ollis (7), Kenneke *et al.* (8), and Glaze *et al.* (9), among others. The mechanism of TCE degradation is known to some extent. After photonic activation of the catalyst two pathways have been envisaged: (i) an oxidative route resulting in the production of chloride ion and trichlorinated intermediates and (ii) a reductive route resulting in the production of dichlorinated compounds. The first one seems to be produced by hydroxyl radical addition followed by oxygen addition and hydrolysis; it is expected to be the major route of chloroalkene degradation. For the second one, a one-electron reduction has been proposed; the resulting radical may protonate, add oxygen, and hydrolyze. The major end products are chloride ion and carbon dioxide. Clearly, TCE is amenable of degradation via hydroxyl radical attack.

Applying a previously developed reactor model and design (1, 2, 10) and the kinetic model presented in Part I (3), this work presents results on the decomposition reaction of a low concentration solution of TCE in water using: (i) oxygen concentration in excess of the stoichiometric demand, (ii) Aldrich (Anatase 99%) titanium dioxide suspended particles, and (iii) near ultraviolet polychromatic radiation. These results provide an intrinsic kinetic formulation for representing the TCE degradation rate.

[1] To whom correspondence should be addressed. E-mail: ACASSANO @SILVA.ARCRIDE.EDU.AR.

0021-9517/97 $25.00

II. MASS BALANCE

In a previous work (3), the following kinetic expression has been obtained:

$$r_P(\mathbf{x}, t) = \alpha_1' \left\{ -\left(\frac{E(R_i, R_j)}{1 + E(R_i, R_j)} \right) + \sqrt{\left(\frac{E(R_i, R_j)}{1 + E(R_i, R_j)} \right)^2 + \frac{\alpha_2'}{C_{mp}} \int_\lambda e_\lambda^a(\mathbf{x}, t)\, d\lambda} \right\} \times \left(\frac{\alpha_{3,i}[R_i]}{1 + E(R_i, R_j)} \right). \quad [1]$$

Equation [1] is valid for a catalytic "particle" inside a suspended solid photocatalytic reactor.

Let us obtain an equation valid for a material point inside the reactor and show how this value should be used for a typical photocatalytic laboratory or bench scale reactor system. We will use a perfectly stirred continuous flow reactor inside the loop of a recirculating system as an example. We will also require that: (i) The tank volume must be larger than the reactor volume ($V_{Tk} \gg V_R$), (ii) The recirculating flow rate should be very high such as changes in concentration per path in the photocatalytic reactor be very small, and (iii) The connecting lines between the tank and the reactor should have a negligible volume. Condition (i) will be convenient to reach a simpler method for the analysis of the experimental results and to facilitate sampling; however, it will render longer experimental runs for an accurate measurement of concentration changes. Condition (ii) will improve uniformity of the solid suspension and also it will be useful to render a simpler, yet very accurate, way of interpreting the experimental data.

As is shown in Appendix A, a rigorous mass balance for this system gives

$$\varepsilon_L \frac{dC_i(\mathbf{x}, t)}{dt} = \frac{V_R}{V_{Tk}} a_V \langle r_{S,i}(\mathbf{x}, t) \rangle_{A_{S,R}} = \frac{V_R}{V_{Tk}} C_{mp} S_g \nu_i \langle r_S(\mathbf{x}, t) \rangle_{A_{S,R}}. \quad [2]$$

In Eq. [2] the catalytic surface area per unit suspension volume has been substituted by the product of the catalyst loading and the catalyst specific surface area: ($a_V = C_{mp} S_g$).

Equation [2] can be integrated with an initial condition:

$$C_i(t = 0) = C_{i,o}. \quad [3]$$

The reaction rate per particle, Eq. [1], must be transformed into an expression valid for a heterogeneous catalytic reactor; i.e., a reaction per unit surface area ($r_S(\mathbf{x}, t)$ [=] mol s^{-1} m^{-2}). Clearly,

$$r_S(\mathbf{x}, t) = \frac{r_P(\mathbf{x}, t)}{a_S}. \quad [4]$$

One can also define

$$\alpha_1 = \frac{\alpha_1'}{a_S}, \quad \alpha_2 = \alpha_2'. \quad [5]$$

Substituting Eq. [1] into Eq. [4] and the result into Eq. [2] and considering that TCE is the only reacting species, we finally get

$$\varepsilon_L \frac{dC_i(t)}{dt} = -\frac{V_R}{V_{Tk}} C_{mp} S_g \alpha_1 \left\{ \left\langle -\left(\frac{\alpha_{3,i} C_i(t)}{1 + \alpha_{3,i} C_i(t)} \right) + \sqrt{\left(\frac{\alpha_{3,i} C_i(t)}{1 + \alpha_{3,i} C_i(t)} \right)^2 + \frac{\alpha_2}{C_{mp}} \int_\lambda e_\lambda^a(\mathbf{x}, C_{mp})\, d\lambda} \right\rangle_{A_{S,R}} \right\} \times \left(\frac{\alpha_{3,i} C_i(t)}{1 + \alpha_{3,i} C_i(t)} \right). \quad [6]$$

Since the catalytic performance has been assumed unchanged during the course of the reaction (chemical, mechanical, and optical catalyst stability has been assumed), the LVREA may be considered independent of time. However, in order to make explicit that it strongly depends on the catalyst loading, this parametric dependence has been clearly stated in Eq. [6]. In this equation, the concentration of the reacting species has been written with a uniform nomenclature (C_i). Assuming that the superficial area per unit reactor volume (a_V) is independent of reactor position and considering that the reactor cross sectional area (A_R) is uniform, Cabrera *et al.* [1] have shown that for the one-dimensional one-directional model (1-Dim–1-Dir Model) is

$$\left\langle -\left(\frac{\alpha_{3,i} C_i(t)}{1 + \alpha_{3,i} C_i(t)} \right) + \sqrt{\left(\frac{\alpha_{3,i} C_i(t)}{1 + \alpha_{3,i} C_i(t)} \right)^2 + \frac{\alpha_2}{C_{mp}} \int_\lambda e_\lambda^a(\mathbf{x}, C_{mp})\, d\lambda} \right\rangle_{A_{S,R}} = \left\langle -\left(\frac{\alpha_{3,i} C_i(t)}{1 + \alpha_{3,i} C_i(t)} \right) + \sqrt{\left(\frac{\alpha_{3,i} C_i(t)}{1 + \alpha_{3,i} C_i(t)} \right)^2 + \frac{\alpha_2}{C_{mp}} \int_\lambda e_\lambda^a(\mathbf{x}, C_{mp})\, d\lambda} \right\rangle_{L_R}. \quad [7]$$

TABLE 1

Reactor, Lamp, and Reflector Characteristics

	Parameter	Value
Reactor	Inside diameter	5.2 cm
	Length	10.0 cm
	Plate thickness	0.38 cm
	Plate radius	2.7 cm
	Reactor volume	212 cm^3
	Total volume	1950 cm^3
Lamp 360 UA-3	Nominal power	360 W
	Diameter	1.9 cm
	Arc length	15.2 cm
Reflector	Parabola characteristic constant	2.5 cm
	Distance from vertex of parabolic reflector to reactor plate	14.8 cm
	Length	22.0 cm

In Eq. [7]

$$\left\langle -\left(\frac{\alpha_{3,i}C_i(t)}{1+\alpha_{3,i}C_i(t)}\right) + \sqrt{\left(\frac{\alpha_{3,i}C_i(t)}{1+\alpha_{3,i}C_i(t)}\right)^2 + \frac{\alpha_2}{C_{mp}}\int_\lambda e_\lambda^a(\mathbf{x}, C_{mp})\,d\lambda}\right\rangle_{L_R}$$
$$= \frac{1}{L_R}\int_0^{L_R}\left\{-\left(\frac{\alpha_{3,i}C_i(t)}{1+\alpha_{3,i}C_i(t)}\right) + \sqrt{\left(\frac{\alpha_{3,i}C_i(t)}{1+\alpha_{3,i}C_i(t)}\right)^2 + \frac{\alpha_2}{C_{mp}}\int_\lambda e_\lambda^a(\mathbf{x}, C_{mp})\,d\lambda}\right\}dx \quad [8]$$

is the reactor length average of the kinetic model expression. Since $C_i(t)$ is uniform throughout, the average procedure is mainly concerned with the LVREA which is a function of position.

From Eqs. [6] and [7], the final working equation to interpret the experimental data will be

$$\varepsilon_L\frac{dC_i(t)}{dt} = -\frac{V_R}{V_{Tk}}C_{mp}S_g\alpha_1\left\{\left\langle -\left(\frac{\alpha_{3,i}C_i(t)}{1+\alpha_{3,i}C_i(t)}\right) + \sqrt{\left(\frac{\alpha_{3,i}C_i(t)}{1+\alpha_{3,i}C_i(t)}\right)^2 + \frac{\alpha_2}{C_{mp}}\int_\lambda e_\lambda^a(\mathbf{x}, C_{mp})\,d\lambda}\right\rangle_{L_R}\right\} \times\left(\frac{\alpha_{3,i}C_i(t)}{1+\alpha_{3,i}C_i(t)}\right). \quad [9]$$

In Eq. [9] $C_i(t)$ and t are experimental data, C_{mp} is a reaction parameter and $\int_\lambda e_\lambda^a(\mathbf{x}, C_{mp})\,d\lambda$ can be computed from lamp, reactor, reflector, and catalyst available information (Table 1). Then, with a nonlinear regression procedure the three kinetic parameters (α_1, α_2, and $\alpha_{3,i}$) can be obtained (see Section V).

III. EXPERIMENTAL

Cabrera *et al.* (1) and Alfano *et al.* (2) developed a special type of photocatalytic reactor that permits a rigorous evaluation of radiation absorption and scattering. With a precise reactor design and working under carefully controlled experimental conditions, this experimental setup can be used to obtain intrinsic kinetic results, i.e. results that are able to provide a local value of the reaction rate and are totally independent of lamp and reactor configurations. Only this type of results can be used for direct scale-up and reactor design purposes. There is one limitation to this statement: in principle these results are valid for the radiation wavelength range under which they were obtained. This is due to the expected dependence of quantum yields with wavelength.

Experimental Setup

Figure 1 presents a schematic representation of the reactor and Fig. 2 shows the whole experimental setup. There are three major components of the system: (i) an irradiating device, (ii) the reactor, and (iii) the recycling system:

Irradiating system. Radiant energy is supplied by a medium pressure, mercury arc lamp having a rated power of 360 W (UA-3 UVIARC®, General Electric (11)). The tubular lamp is placed at the focal axis of a cylindrical reflector of the parabolic cross section. The reflector was made with a specularly finished aluminum sheet having Alzac® treatment (12). The principal dimensions are indicated in Table 1. The lamp and the reflector are housed in a metallic

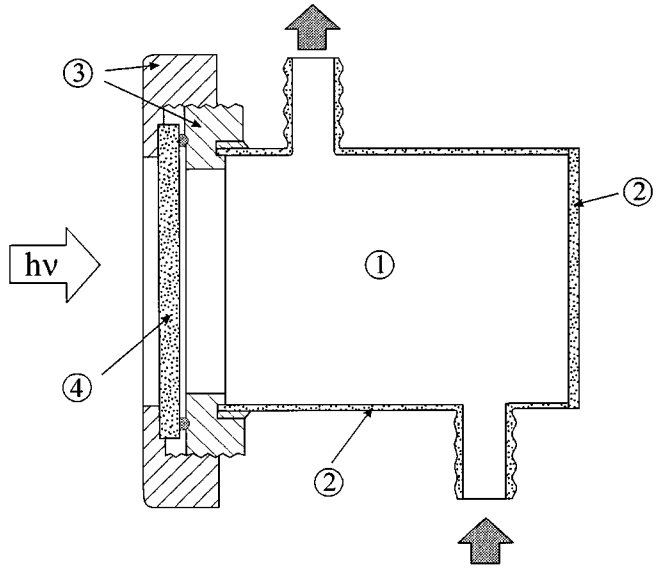

FIG. 1. Details of the experimental reactor: ① reaction space; ② Pyrex glass; ③ nylon piece; ④ Pyrex window.

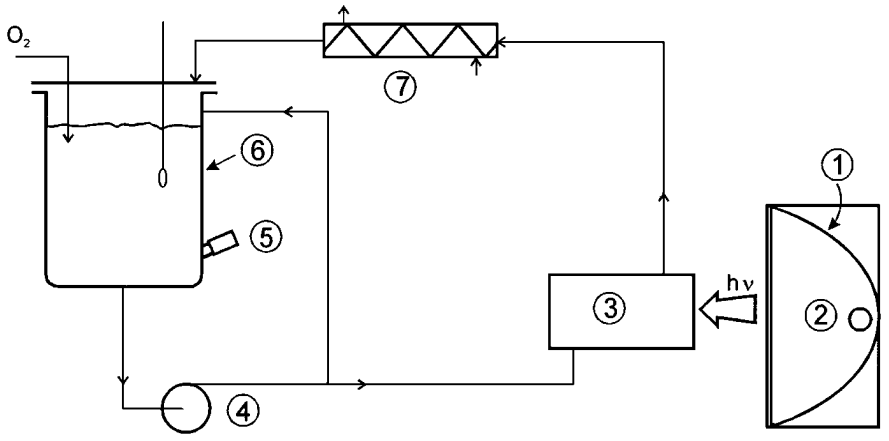

FIG. 2. Flow sheet of the experimental device: ① parabolic reflector; ② UV lamp; ③ reactor; ④ pump; ⑤ liquid sampling; ⑥ storage tank; ⑦ heat exchanger.

box that provided accurate positioning of both components. Proper operation of the lamp is controlled by means of a V-A-W meter (Clarke-Hess Model 255).

Reactor. Its dimensions are given in Table 1. It was made of Pyrex® glass. The front side is closed by a circular plate made of Pyrex® glass. The interior side of this plate was made of ground glass. A Viton® O-ring provides the hydraulic sealing. Both the reactor and the radiation emission system are mounted on a triangular optical bench (Ealing) which permits an accurate positioning of the former with respect to the irradiating device. The whole setup (reactor–lamp–reflector) is covered by a metallic box that was painted black and is connected to an exhaust system. A shutter allows us to isolate the reactor from the lamp; it is in place during the time required by the lamp and the reactor to reach stable operating conditions (temperature, flow rate, etc.); when it is removed the reaction starts.

Recycling system. As indicated in Fig. 2 the reactor operates as a perfectly stirred, continuous flow tank, inside the loop of a batch recirculating system. The experimental device is completed with a storage tank of 2500 cm^3 made of Pyrex® glass that has a gas inlet for oxygen saturation. The system operates with just one gas inlet for oxygen that generates a small overpressure on the gas–liquid interface; the recirculating flow in the vessel facilitates good mixing conditions; in this way the oxygen consumed by the reaction is permanently replenished. No gas outlet is provided in order to avoid TCE and CO_2 stripping. The storage tank also has a thermometer and two sampling systems: one for the liquid phase and another for the gas phase (head space). High recirculating flow rate to and from the reactor is provided by means of an all glass and Teflon® centrifugal pump (Jobling Glass) which is operated by means of a variable speed motor. The liquid flow rate must be high in order to ensure good mixing conditions in the whole reacting system. Between the reactor outlet and the storage tank there is a heat exchanger made of glass that is connected to a thermostatic bath (Lauda K2R). It ensures reaction operating conditions at 20°C.

Optical properties of the reflector and the glass, as well as detailed information about the lamp performance (spectral distribution and absolute value of its output power), must be known.

The design must assure the following operating conditions: (i) very good reproducibility in the radiation flux arriving at the reactor window, (ii) very good mixing conditions in the tank, (iii) differential conversion per pass in the photoreactor, (iv) minimum volume in the connecting lines, and (v) absence of gas leaks everywhere.

It must be stressed that good mixing conditions are a requirement of the model equations. They are necessary not only for the proper simplifications of the mass balance equation but also to make sure that mass transport limitations are absent during the reactor operation and that the catalyst suspension has uniform concentration in the reacting space.

Experimental Procedure

The experimental operating conditions are indicated in Table 2. The reactant mixtures (very low concentrations of TCE (99.9% by GLC, Carlo Erba, RSE) in ultra pure water (Barnstead, 18 MΩ; filtered 0.2 μm)) was prepared from a stock solution of water saturated with TCE at 293 K (6 h of equilibration time; saturation concentration at 293 K = 1076 ppm). Approximately 2000 cm^3 of water, circulating at a high flow rate in the closed loop, were saturated with pure oxygen by intense bubbling during 30 min at 293 K. The desired amount of TCE taken from the stock solution was then added to the tank. The whole system was tightly closed and oxygen was allowed to enter into the tank while liquid recirculation was established once more. A sample from the gas phase in the tank (400 μL) was taken and analyzed in the gas chromatograph at time intervals of 10 min. When this

TABLE 2

Experimental Operating Conditions

Catalyst	Aldrich titanium dioxide (>99% anatase) sp. surf. area: 9.6 $m^2\ g^{-1}$ nominal diameter: 150–200 nm concn.: (0.1, 0.2, and 1.0) $\times 10^{-3}$ g cm^{-3}
Reactant solution (in water)	Trichloroethylene Carlo Erba RSE MW = 131.36 g mol^{-1} concn.: (0.084 to 0.55) $\times 10^{-6}$ mol cm^{-3} initial pH: 6
Oxidant	Oxygen, saturated at 293 K
Temperature	293 K
Lamp	GE UA-3 Uviarc 360 W Hg medium pressure P (295–405 nm) = 6×10^{-5} einstein s^{-1}
Radiation flux at reactor entrance (295–405 nm)	1.14×10^{-7} einstein $cm^{-2}\ s^{-1}$

concentration was constant, a sample from the liquid phase (30 cm^3) was analyzed in the gas chromatograph (see below) and this result was considered the "feed" concentration.

Through the sampling port, the required amount of catalytic suspension was added to the tank and recirculation of the liquid was maintained for 1 h. The catalyst was suspended in a small volume of water and added to the sample port by means of a specially constructed syringe. Immediately after, the oxygen feed was stopped and the fluid recirculation turned off. The system was maintained in this condition for 17 h to ensure that the "dark" adsorption equilibrium had been reached. Afterwards, the oxygen feed, the recirculating pump, the temperature control, and the UV lamp (the shutter of the irradiating system still blocked the light) were turned on. Samples from the gas phase were taken once more until a constant concentration was observed. After 2 h the whole system was equilibrated. A new liquid sample was taken which was considered the "initial" concentration. In this sample, chloride ion and carbonates were also analyzed by ion-chromatography. At this moment the lamp housing shutter was removed and the reactor radiation entrance window was illuminated, indicating the starting of the reaction. It must be noted that "feed" TCE concentration and "initial" TCE concentration were not equal. Every run lasted 8 h with sampling of the liquid (30 cm^3) taken every 2 h. Between different runs the complete reaction system was carefully washed to eliminate small amounts of catalyst that usually stick to the reactor walls, the centrifugal pump, the glass heat exchanger, and the connecting tubes.

Analyses were made in the following way: (i) TCE by GC (Hewlett-Packard Model 5890) with FID detectors and a 60-cm long Porapak Q-S column. They were made by duplicate, with the Head Space technique (9), using samples of 10 cm^3 each, equilibrated during 45 min at 303 K and injecting 400 μL from the gas phase. (ii) Chloride ion and carbon dioxide by means of ion chromatography (Dionex 2020I) with conductivity detectors. Chloride ion required a HPIC-AS2 Anion Separator and a ASC-2 Anion Suppresor columns, and carbonates (obtained from transformation of the dissolved carbon dioxide with sodium hydroxide) a HPICE AS1 column, all of them from Dionex.

Optical properties of the titanium dioxide suspension (absorption and scattering coefficients) must be known. They were taken from a recent work (13).

The results will be analyzed in terms of changes in reactant concentration. During the runs, as a consequence of the HCl formation, the pH changes from its initial value (pH = 6) to rather acidic conditions (pH $\cong$ 4). Under these circumstances, the carbon dioxide determination by ion chromatography does not represent the equivalent of the total amount produced by the photocatalytic reaction; it is just that part of it that remains in the aqueous solution. Another part of it may have been transferred to the gas phase. Hence, one should not expect to be able to have a closed mass balance with respect to carbon dioxide. Moreover, chloride ion is not generated at a rate that corresponds to the stoichiometric ratio (with respect to TCE), indicating the existence of reaction intermediates. Closing the mass balance with respect to the TCE/chloride ion relationship was obtained with very long runs (6 to 8 h after the TCE concentration achieved a negligible value).

IV. PRELIMINARY RESULTS

Dark Adsorption

During the preparation of the reaction mixture it was clearly observed that the "feed" concentration was not equal to the "initial" concentration. The difference was attributed to adsorption of the TCE by the solid catalyst and some parts of the reactor setup and to absorption by the Teflon parts of the centrifugal pump and the top of the storage tank. A detailed study of the adsorption isotherms in order to characterize this phenomenon and its characteristic parameters (14–16) is a task that lies outside the scope of this research. What we really need for our work is a precise knowledge of the amount of TCE that remains in the bulk of the liquid phase. This information is needed for different catalyst and substrate concentrations within the explored range of the variables used along the kinetic study. This information should be enough to isolate from the observed changes in TCE concentration those corresponding exclusively to the photocatalytic degradation.

The experimental procedure was exactly the same that was described for the preparation of the initial conditions for a TCE degradation run. Temperature was maintained constant at 293 K. Two different sets of experiments were carried out: (i) adsorption runs without subsequent degradation and (ii) adsorption runs that were part of the preparation of the initial conditions for a degradation run. In both

TABLE 3

Dark Adsorption Experiments for TCE

$TiO_2 \times 10^3$ (g cm^{-3})	$C_{TCE,o} \times 10^6$ (mol cm^{-3})	$C_{TCE,e} \times 10^6$ (mol cm^{-3})	Type of experiment
0.1	0.158	0.084	Degradation
0.1	0.164	0.107	Adsorption
0.1	0.297	0.240	Adsorption
0.1	0.358	0.265	Degradation
0.1	0.614	0.455	Adsorption
0.1	0.641	0.525	Degradation
0.2	0.155	0.105	Degradation
0.2	0.171	0.126	Adsorption
0.2	0.374	0.287	Degradation
0.2	0.395	0.305	Adsorption
0.2	0.681	0.512	Adsorption
0.2	0.748	0.551	Degradation
1.0	0.176	0.136	Degradation
1.0	0.228	0.171	Adsorption
1.0	0.283	0.211	Degradation
1.0	0.361	0.299	Adsorption
1.0	0.604	0.452	Adsorption
1.0	0.746	0.503	Degradation

types of experiments the concentration of TCE was varied from approximately 0.15×10^{-6} to 0.75×10^{-6} mol cm^{-3} and catalyst loads were 0.1×10^{-3}, 0.2×10^{-3}, and 1.0×10^{-3} g cm^{-3}. Table 3 presents a summary of the adsorption experiments. For different catalyst mass concentrations the initial and equilibrium molar concentrations of TCE are shown. The results correspond to the two different types of experiments described above.

A linear regression can be applied to these data for each catalyst concentration. Results from the linear regression and the experimental data are plotted in Fig. 3 that correspond to a representation of $C_{TCE,o}$ versus $C_{TCE,e}$. The line of slope equal to 1 (no adsorption) is also plotted; clearly, all experimental points must lie above this straight line. For each catalyst concentration a different slope was obtained. However, the differences among them are relatively small. The numerical value of the slope corresponding to a single straight line is $s = 1.335$. Then, the percentage reduction of the TCE concentration due to adsorption in the dark, relative to the TCE initial concentration can be expressed as

$$A_{TCE}\,(\%) = \frac{C_{TCE,o} - C_{TCE,e}}{C_{TCE,o}} \times 100 = \frac{s-1}{s} \times 100. \quad [10]$$

Substituting into Eq. [10] the value of s obtained from the linear regression of the adsorption data one can conclude that the extent of these changes in concentration due to different sinks is about 25%. Two things were carefully verified: (i) these changes in concentration were not due to leaks in the system and (ii) only a very small amount of these changes can be attributed to adsorption by titanium dioxide.

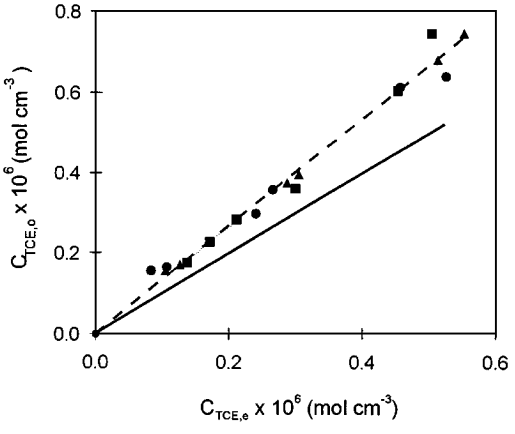

FIG. 3. Dark adsorption of TCE for different catalyst loading. Keys: (●) $C_{mp} = 0.1 \times 10^{-3}$ g cm^{-3}; (▲) $C_{mp} = 0.2 \times 10^{-3}$ g cm^{-3}; (■) $C_{mp} = 1.0 \times 10^{-3}$ g cm^{-3}; (———) s = 1.

Adsorption under Illuminated Conditions

We have been informed (17) that in some cases after illumination, an increase in adsorption has been observed (some sort of photoenhanced adsorption). When the system returns to the dark conditions, the extrapolated initial concentration of the substrate (with due account of the photocatalytic degradation) is practically restored. A special degradation experiment was designed to verify this possibility for the TCE (water)–titanium dioxide system. Preparation of the run was done as described before. The maximum catalyst concentration (1.0×10^{-3} g cm^{-3}) was used. The "feed" concentration was 0.34×10^{-6} mol cm^{-3}. The "initial" concentration, after equilibration, was 0.266×10^{-6} mol cm^{-3}. After 2 h of photocatalytic degradation the shutter of the irradiating system was put on. The system was kept in the dark for 2 h. The whole procedure was then repeated: 2 h of irradiation with the shutter off, followed by 2 h under dark conditions. At the end of each time interval samples were taken from the tank. The results are described in Table 4. These results indicate that: (i) During the first 120 min ($t_1 - t_0$), having the reactor under illumination (shutter off), the reaction

TABLE 4

Photo-Adsorption for TCE onto TiO_2 (Aldrich)

	TCE concentration[a] $\times 10^6$ (mol cm^{-3})				
Time (h)	UV radiation	Dark	UV radiation	Dark	Reaction conversion (%)
0	0.266				0.0
2	0.163	0.163			38.7
4		0.162	0.162		39.1
6			0.106	0.106	60.1
8				0.098	63.1

[a] For $C_{TCE,o} = 0.340 \times 10^{-6}$ mol cm^{-3}.

conversion $\{X_{TCE}(t_1) = [(C_{TCE,o} - C_{TCE,t_1})/C_{TCE,o}] \times 100\}$ was 38.7%. (ii) During the first dark period (120 min) there is an "increment" in conversion (decrease in TCE concentration) of 0.4%. (iii) During the second degradation period ($t_2 - t_1 = 120$ min) with the light on, conversion $\{X_{TCE}(t_2) = [(C_{TCE,o} - C_{TCE,t_2})/C_{TCE,o}] \times 100\}$ increased from 39.1 to 60.1%. (iv) During the second dark period conversion was changed from 60.1 to 63.1%. If photoadsorption is important one should expect an increase in TCE concentration during the dark period (a negative conversion). Results are in the opposite direction and, moreover, variations in concentrations (that cause conversions of 0.4 and 3%) are within the experimental error. One can conclude that if radiation-enhanced adsorption exists, it could not be detected in our experimental setup; either because it was not present or because the sampling and analysis were not sufficiently fast to detect these changes.

V. KINETIC PARAMETERS EVALUATION

In a previous work we developed:

1. A photocatalytic reactor and reactor model that permits the precise evaluation of radiation absorption and scattering (1, 2). The radiation field is analyzed in terms of a one-dimensional one-directional radiative transfer model. With this approach the local volumetric rate of energy absorption (LVREA) at every point inside the reactor can be known. The concentration field is modeled as one-dimensional. The same reactor has been used here.

2. A special procedure to measure radiation absorption and scattering coefficients of solid titanium dioxide suspensions in water providing information about the parameters that are required to solve the RTE (13). Almost conventional spectrophotometric measurements, as well as forward scattering measurements (obtained by means of an integrating sphere), were combined with a radiation transport model for the spectrophotometer cell and a nonlinear multiparameter estimator. In this way, the computer code provided the values of the optical coefficients.

3. An extension of Turchi and Ollis' (6) kinetic scheme for photocatalytic reactions involving hydroxyl radical attack (3). In this work the precise evaluation of the photon–solid interaction and the proper knowledge of the LVREA $[e^a_\lambda(\mathbf{x}, C_{mp})]$ were incorporated into the kinetic expression. The final result can be applied to any photocatalytic reactor regardless its irradiation level.

As explained in Section IV, all experiments were made for TCE concentrations between 0.15×10^{-6} and 0.75×10^{-6} mol cm^{-3}, and three different levels of catalyst concentration were used: 0.1×10^{-3}, 0.2×10^{-3}, and 1.0×10^{-3} g cm^{-3}. Experiments were performed at three different irradiating conditions. A neutral density mechanical screen was interposed between the lamp and the reactor. In this way the irradiation level was varied in the following sequence: 100, 30, and 10%. These runs were made for $C_{mp} = 0.2 \times 10^{-3}$ g cm^{-3} and initial concentrations of (0.20 to 0.29) $\times 10^{-6}$ mol cm^{-3}.

According to these results the experimental data produced in our work can be evaluated in terms of Eq. [9], where the parameters (α_1, α_2, and $\alpha_{3,i}$) were obtained using the Levenberg–Marquardt algorithm (18).

The numerical algorithm receives the following information: (i) TCE concentration–time relationships resulting from the integration of Eq. [9]; these results are obtained with a Runge–Kutta integration procedure. (ii) Results of the integration of the RTE to incorporate values of the LVREA into Eq. [9]; the RTE is integrated using the Discrete Ordinate Method (19). For polychromatic radiation the local values of e^a_λ must be integrated over the wavelength range of interest and, afterwards, integrated once more over the reactor length to obtain the volume averaged rate of reaction (see Eq. [9]). (iii) Experimental TCE-time information. The parameter evaluator searches with an optimization technique the minimum differences between experimental values and theoretical predictions.

Table 5 gives the values of the three kinetic parameters α_1, α_2, and $\alpha_{3,i}$. Figures 4a, b, and c present the experimental data and model prediction results (solid lines) of the time evolution of TCE concentration for three different catalyst concentrations. In addition, each figure also shows the experimental and theoretical results for three different TCE initial concentrations. Clearly the reaction rate is faster when the TCE concentration is higher and it also increases when the catalyst concentration is increased. In Figs. 5a, b, and c we represent the results obtained for changes in the boundary condition: the solid line corresponds to the model and the squares to the experimental data when the radiation flux at the wall of radiation entrance was varied as explained before.

Good agreement between model predictions and experimental points can be observed. Only for very low concentrations of TCE (smaller than 0.05×10^{-6} mol cm^{-3}) is the percentage deviation somewhat significant. This is surely due to errors in the analytical technique for measuring TCE in the liquid sample ("head space" combined with FID detectors). For TCE concentrations larger than 0.18×10^{-6} mol cm^{-3}, the percentage error is never larger than 17%.

Looking at these results and considering the theoretical background provided by Alfano *et al.* (3), one can take the

TABLE 5

Numerical Values for the Kinetic Constants

Kinetic constant	α_1	α_2	$\alpha_{3,i}$
Units	(mol cm^{-2} s^{-1})	(g s einstein^{-1})	(cm^3 mol^{-1})
Values	2.46×10^{-8}	1.57×10^{11}	6.42×10^{6}

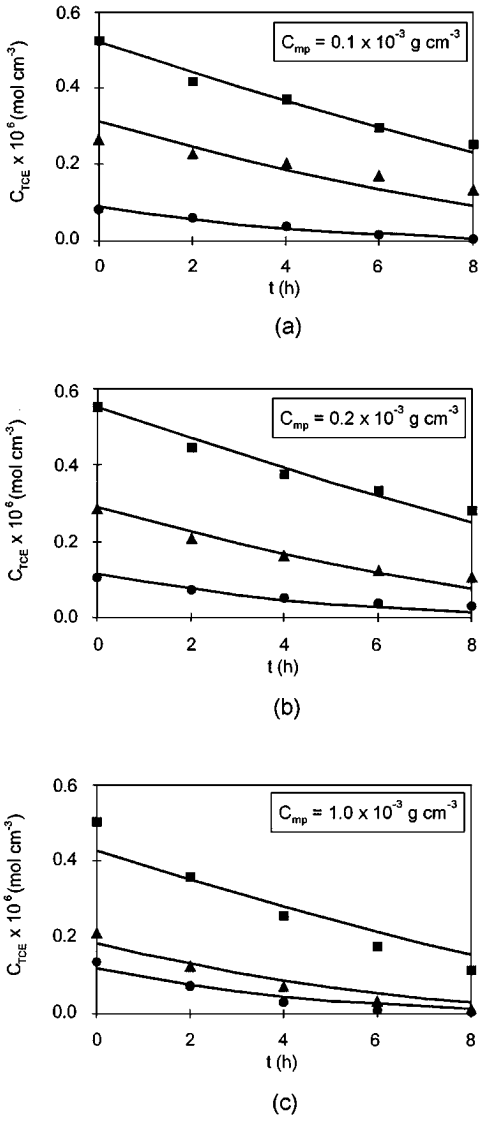

FIG. 4. Trichloroethylene concentration vs time for different catalyst concentrations. Irradiation level: 100%. (a) $C_{mp} = 0.1 \times 10^{-3}$ g cm^{-3}, (b) $C_{mp} = 0.2 \times 10^{-3}$ g cm^{-3}, and (c) $C_{mp} = 1.0 \times 10^{-3}$ g cm^{-3}. Keys: (———), kinetic model; (●, ▲, ■), experimental points.

following ratio:

$$\frac{\alpha_2}{C_{mp}} \int_{\lambda} e_{\lambda}^{q}(\mathbf{x}, t)\, d\lambda \Bigg/ \left(\frac{\alpha_{3,i} C_i(t)}{1 + \alpha_{3,i} C_i(t)} \right)^2, \quad i = \text{TCE}. \quad [11]$$

For example, for a catalyst mass concentration of 1.0×10^{-3} g cm^{-3} this ratio varies from 9.4×10^{7} when $x = 0$ and $C_i\ (t = 0) = 0.136 \times 10^{-6}$ mol cm^{-3} to 1.0×10^{-2} when $x \cong 5$ cm and $C_i\ (t = 8\,\text{h}) = 0.0024 \times 10^{-6}$ mol cm^{-3}. It can be seen that this ratio is modified by 10 orders of magnitude. According to the quoted reference the effect of the LVREA on the reaction rate will vary from the square root dependence to the linear dependence. All this change will occur in just the first half of the reactor length.

The proposed kinetic model not only accounts for the two limiting cases for the reaction rate dependence with the absorbed radiation intensities (linear and square root dependence); it also can be applied to all the intermediate conditions that surely exist inside the reactor from one extreme to the other. For example, when $x \cong 2.7$ cm, the ratio indicated by Eq. [11] is $\cong 1$; none of the limiting cases will apply. Then, to properly describe the reactor behavior at any of its points, the complete equation, Eq. [9], must be used.

It should be noted that in practical situations a polluted stream will normally have a mixture of different hydrocarbons instead of a single component in ultrapure water. In these cases the system will have

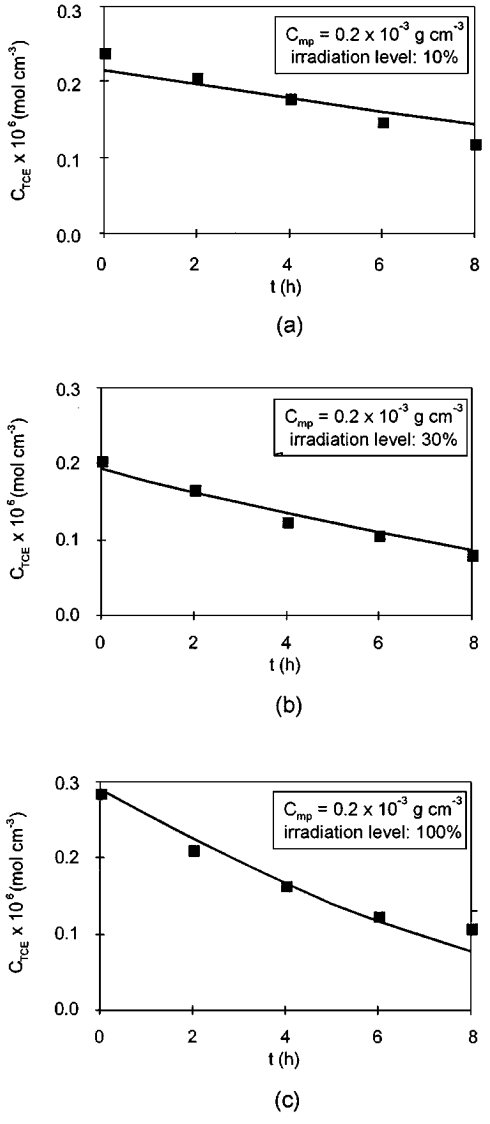

FIG. 5. Trichloroethylene concentration vs time for different irradiating conditions. $C_{mp} = 0.2 \times 10^{-3}$ g cm^{-3}. Irradiation level: (a) 10%, (b) 30%, and (c) 100%. Keys: (———), kinetic model; (■), experimental points.

complex interactions of the type hydrocarbon–hydrocarbon, hydrocarbon–catalytic surface, and inorganic salts–catalytic surface that are much more difficult to model. In these cases, very likely, the reaction evolution will have to be represented and monitored with a "single concentration" comprising the whole set of existing pollutants, such as a measure of the total organic carbon. With this approach, the kinetic modeling could be again reduced to a rather simple representation. Moreover, following TOC values, it is easier to ensure that the achieved pollution remediation includes the destruction of the original compounds and the reaction intermediates.

CONCLUSIONS

A kinetic model previously developed has been used to analyze the kinetics of the photocatalytic degradation of trichloroethylene. The model was applied to the whole time evolution of the decomposition reaction. The model with three constants (theoretically rationalized) permits a good representation of the reaction evolution in a rather wide range of TCE concentrations.

Computed results indicated that inside the reactor one can have regions of high irradiation rates coexisting with other regions of very low irradiation rates. One can conclude that it is very difficult to conceive a reactor where only one kinetic regime will exist. The developed model accounts, in a single equation, for all irradiation levels. Obviously, it includes the transition regime in passing from one limiting situation to the other.

The developed reactor model also provides a rigorous expression for obtaining intrinsic kinetic data from laboratory or bench scale photocatalytic reactors. The mathematical analysis of the formulation provides design and operating conditions that must be fulfilled by experimental reactors in order to produce kinetic information that will be independent of the laboratory conditions and/or reactor configuration.

APPENDIX A: THE REACTOR MODEL

A local mass balance for the i-component in the liquid is (20)

$$\frac{\partial C_i(\mathbf{x}, t)}{\partial t} + \nabla \cdot \mathbf{N}_i = 0. \qquad [A.1]$$

In Eq. [A.1] C_i and $\mathbf{N}_i$ are the molar concentration and molar flux of component i, respectively. This equation can be integrated over the whole liquid volume of the system ($V_{L,T}$) that, in principle, is different from the total volume of the suspension ($V_{Tot} = V_{Tk} + V_R$):

$$\int_{V_{L,T}} \frac{\partial C_i(\mathbf{x}, t)}{\partial t}\, dV + \int_{V_{L,T}} \nabla \cdot \mathbf{N}_i\, dV = 0. \qquad [A.2]$$

Applying the Reynolds' transport theorem to the first term,

$$\int_{V_{L,T}} \frac{\partial C_i(\mathbf{x}, t)}{\partial t}\, dV = \frac{\partial}{\partial t} \int_{V_{L,T}} C_i(\mathbf{x}, t)\, dV - \int_{A_{L,T}} C_i(\mathbf{x}, t)\mathbf{w}_L \cdot \mathbf{n}_L\, dA. \qquad [A.3]$$

In Eq. [A.3] $\mathbf{w}_L$ is the velocity of the liquid interface and $\mathbf{n}_L$ is the outwardly directed unit normal vector to the liquid phase. The second integral can be divided in two parts: (i) one comprising the liquid volume of the reactor and (ii) the other comprising the liquid volume of the tank. Considering that the total interfacial area of the liquid must be equal to the total interfacial area of the solid particles ($A_{L,T} = A_{S,T}$),

$$\int_{V_{L,T}} \frac{\partial C_i(\mathbf{x}, t)}{\partial t}\, dV = V_{L,R} \frac{d}{dt} \langle C_i(\mathbf{x}, t) \rangle_{V_{L,R}} + V_{L,Tk} \frac{dC_i(t)}{dt} - \int_{A_{S,T}} C_i(\mathbf{x}, t)\mathbf{w}_{S,T} \cdot \mathbf{n}_{S,T}\, dA. \qquad [A.4]$$

In Eq. [A.4], $\langle C_i(\mathbf{x}, t) \rangle_{V_{L,R}}$ is the reactor liquid volume averaged concentration of component i, $\mathbf{w}_{S,T}$ is the velocity of the liquid–solid particles interface, and $\mathbf{n}_{S,T}$ is the outwardly directed unit normal vector to the liquid–solid particle interface. In the well-stirred tank, since there is no chemical reaction, $C_i(\mathbf{x}, t)$ is uniform and can be taken out of the volume integral.

In turn, using the divergence theorem and the definition of the molar flux, the right-hand side of Eq. [A.2] can be written as

$$\int_{V_{L,T}} \nabla \cdot \mathbf{N}_i\, dV = \int_{A_{S,T}} [\mathbf{J}_i(\mathbf{x}, t) + C_i(\mathbf{x}, t)\mathbf{v}] \cdot \mathbf{n}_{S,T}\, dA. \qquad [A.5]$$

Once more we have considered that $A_{L,T} = A_{S,T}$. In Eq. [A.5] $\mathbf{v}$ is the molar averaged liquid velocity. Substituting Eqs. [A.4] and [A.5] into Eq. [A.2],

$$V_{L,R} \frac{d}{dt} \langle C_i(\mathbf{x}, t) \rangle_{V_{L,R}} + V_{L,Tk} \frac{dC_i(t)}{dt} = -A_{S,T} \langle [\mathbf{J}_i(\mathbf{x}, t)] \cdot \mathbf{n}_{S,T} \rangle_{A_{S,T}} + \int_{A_{S,T}} C_i(\mathbf{x}, t)\, [\mathbf{w}_{S,T} - \mathbf{v}] \cdot \mathbf{n}_{S,T}\, dA. \qquad [A.6]$$

In Eq. [A.6] $\langle [\mathbf{J}_i(\mathbf{x}, t)] \cdot \mathbf{n}_{S,T} \rangle_{A_{S,T}}$ is the total liquid–solid particles interface averaged molar diffusive flux of component i. The second term of the right-hand side of Eq. [A.6] is zero because $[\mathbf{w}_{S,T} - \mathbf{v}] = 0$; this is so because, according to the nonslipping condition at the liquid–solid interface,

both velocities are equal. Clearly, the molar diffusive flux at the liquid–solid interface, must be equal to the reaction rate at the liquid–solid interface:

$$A_{S,T}\langle \mathbf{J}_i \cdot \mathbf{n}_{S,T}\rangle_{A_{S,T}} = A_{S,R}\langle \mathbf{J}_i \cdot \mathbf{n}_{S,T}\rangle_{A_{S,R}} = -A_{S,R}\langle \nu_i r_S\rangle_{A_{S,R}}. \quad [A.7]$$

In Eq. [A.7] the molar flux at the solid–liquid interface is different from zero only at the permeable solid–liquid interface, i.e. the solid–liquid interface of the reactor where there is chemical reaction. This means that this flux is different from zero only at $A_{S,R}$. Substituting Eq. [A.7] into Eq. [A.6] and dividing by V_{Tk},

$$\varepsilon_L \frac{V_R}{V_{Tk}} \frac{d}{dt}\langle C_i(\mathbf{x}, t)\rangle_{V_{L,R}} + \varepsilon_L \frac{dC_i(t)}{dt} = \frac{V_R}{V_{Tk}} a_V \langle \nu_i r_S(\mathbf{x}, t)\rangle_{A_{S,R}}. \quad [A.8]$$

In Eq. [A.8] the definitions

$$\frac{V_{L,R}}{V_R} = \frac{V_{L,Tk}}{V_{Tk}} = \varepsilon_L, \quad [A.9]$$

$$A_{S,R} = a_V V_R \quad [A.10]$$

have been used, where ε_L is the liquid hold-up in the system that is uniform throughout, and a_V is the catalytic surface area per unit suspension volume.

Since $V_R/V_{Tk} \ll 1$ (a design conditions),

$$\varepsilon_L \frac{dC_i(t)}{dt} = \frac{V_R}{V_{Tk}} a_V \langle \nu_i r_S(\mathbf{x}, t)\rangle_{A_{S,R}} = \frac{V_R}{V_{Tk}} a_V \langle r_{S,i}(\mathbf{x}, t)\rangle_{A_{S,R}}. \quad [A.11]$$

This is Eq. (2) of the main body of the paper.

APPENDIX B: NOTATION

A	area, m^2
A_{TCE}	extent of dark adsorption for TCE onto TiO_2, dimensionless
a_S	particle surface area, m^2 particle^{-1}
a_V	catalyst surface area per unit suspension volume, m^2 m^{-3}
C	molar concentration, mol m^{-3}
C_m	mass concentration, g m^{-3}
e^a	local volumetric rate of radiant energy absorption, einstein m^{-3} s^{-1}
$E(R_i, R_j)$	$\alpha_{3,i}[R_i] + \sum_{\substack{j=1 \\ (j\neq i)}}^{n} \alpha_{3,j}[R_j]$, function defined in Eq. [3] in Alfano *et al.* (3), dimensionless
$\mathbf{J}_i$	molar diffusion flux, mol m^{-2} s^{-1}
L	length, m
$\mathbf{N}$	molar flux, mol m^{-2} s^{-1}
$\mathbf{n}_L$	unit normal vector to the liquid phase, dimensionless
$\mathbf{n}_S$	unit normal vector to the liquid-solid particles interface, dimensionless
r_P	reaction rate per particle, mol particle^{-1} s^{-1}
r_S	heterogeneous reaction rate, mol m^{-2} s^{-1}
s	slope (see Eq. 10), dimensionless
S_g	specific surface area, m^2 g^{-1}
t	time, s
$\mathbf{v}$	molar average liquid velocity, m s^{-1}
V	volume, m^3
$\mathbf{x}$	axial coordinate, m
X_{TCE}	reactor conversion, dimensionless
$\mathbf{w}_L$	velocity of the liquid interface, m s^{-1}
$\mathbf{w}_S$	velocity of the liquid-solid particles interface, m s^{-1}

Greek Letters

α_1	kinetic parameter defined in Eq. [5], mol m^{-2} s^{-1}
α_1'	kinetic parameter defined in Eq. [3] in Alfano *et al.* (3), mol s^{-1} particle^{-1}
α_2	kinetic parameter defined in Eq. [5], g s einstein^{-1}
α_2'	kinetic parameter defined in Eq. [15] in Alfano *et al.* (3), g s einstein^{-1}
$\alpha_{3,i}$	kinetic parameter defined in Eq. [A.8] in Alfano *et al.* (3), m^3 mol^{-1}
ε	holdup, dimensionless
λ	wavelength, nm
ν_i	i component stoichiometric coefficient

Subscripts

e	equilibrium
i	relative to species i
L	denotes reactor length or liquid phase
P	indicates a particle property
R	indicates a reactor property
S	indicates a solid property
T	denotes total value
TCE	trichloroethylene
Tk	indicates a tank property
Tot	total volume of the suspension
λ	indicates a dependence on wavelength
o	indicates initial conditions

Special Symbols

$\langle\ \rangle$	indicates average value
[ ]	concentration

ACKNOWLEDGMENTS

The authors are grateful to Consejo Nacional de Investigaciones Científicas y Técnicas (PID-201-1006) and to Universidad Nacional del Litoral (CAI+D-008-063 and 33-174) for their support to produce this work. Special mention is made to Deutsche Gessellschaft für Technische Zusammenarbeit (GTZ) GmbH for an Equipment Grant under Program PN 87.2061.7-02.300/9357. Thanks are also given to Eng. Claudia Romani for technical assistance and Mrs. Silvana Wagner for helping in editing this manuscript.

REFERENCES

1. Cabrera, M. I., Alfano, O. M., and Cassano, A. E., *Ind. Eng. Chem. Res.* **33**, 3031 (1994).
2. Alfano, O. M., Negro, A. C., Cabrera, M. I., and Cassano, A. E., *Ind. Eng. Chem. Res.* **34**, 488 (1995).
3. Alfano, O. M., Cabrera, M. I., and Cassano, A. E., *J. Catal.* **172**, 370 (1997).
4. Serpone, N., and Pellizetti, E., "Photocatalysis: Fundamentals and Applications." Wiley, New York, 1989.
5. Ollis, D. F., and Al-Ekabi, H., "Photocatalysis Purification and Treatment of Water and Air." Elsevier Science, New York, 1993.
6. Turchi, C. S., and Ollis, D. F., *J. Catal.* **122**, 178 (1990).
7. Pruden, A. L., and Ollis, D. F., *J. Catal.* **82**, 404 (1983).
8. Kenneke, J. F., Ferry, J. L., and Glaze, W. H., *in* "Photocatalytic Purification and Treatment of Water and Air" (D. F. Ollis and H. Al-Ekabi, Eds.), p. 179. Elsevier Science, New York, 1993.
9. Glaze, W. H., Kenneke, J. F., and Ferr, J. L., *Env. Sci. Technol.* **27**, 177 (1993).
10. Cabrera, M. I., Alfano, O. M., and Cassano, A. E., *Ind. Eng. Chem. Res.* **34**, 500 (1995).
11. General Electric Co., technical bulletin, "Uviarc (Photochemical) Lamps LS-104," 1959.
12. Koller, L. R., "Ultraviolet Radiation," 2nd ed., Wiley, New York, 1966.
13. Cabrera, M. I., Alfano, O. M., and Cassano, A. E., *J. Phys. Chem.* **100**, 20043 (1996).
14. Cunninngham, J., and Srijaranai, S., *J. Photochem. Photobiol. A: Chem.* **58**, 361 (1991).
15. Cunninngham, J., and Sedlak, P., *in* "Photocatalytic Purification and Treatment of Water and Air" (D. F. Ollis and H. Al-Ekabi, Eds.), p. 67. Elsevier Science, New York, 1993.
16. Cunninngham, J., Al-Sayyed, G., and Srijaranai, S., *in* "Aquatic and Surface Photochemistry" (G. Helz, R. Zepp, and D. Crosby, Eds.), Chap. 22, p. 317. Lewis, Boca Raton, FL, 1994.
17. Sclafani, A., personal communication, 1994.
18. Marquardt, D. W., *J. Soc. Indust. Appl. Math.* **11**, 431 (1963).
19. Duderstadt, J. J., and Martin, R., "Transport Theory." Wiley, New York, 1979.
20. Slattery, J. C., "Momentum, Energy and Mass Transfer in Continua." McGraw–Hill, New York, 1972.